KIRCHHOFF PRE-STACK DEPTH SCALAR MIGRATION OF COMPLETE WAVE FIELD USING THE PREVAILING-FREQUENCY APPROXIMATION OF THE COUPLING RAY THEORY

VÁCLAV BUCHA

Department of Geophysics, Faculty of Mathematics and Physics, Charles University, Ke Karlovu 3, 121 16 Praha 2, Czech Republic. bucha@seis.karlov.mff.cuni.cz

(Received October 6, 2022; accepted February 6, 2023)

ABSTRACT

Bucha, V., 2023. Kirchhoff pre-stack depth scalar migration of complete wave field using the prevailing-frequency approximation of the coupling ray theory. *Journal of Seismic Exploration*, 32: 105-129.

Many ray tracers based on the anisotropic ray theory yield distorted results or even collapse when shear waves propagating in inhomogeneous weakly anisotropic models are computed. The coupling ray theory provides more accurate polarizations and travel times of S-waves in inhomogeneous models with weak anisotropy than the anisotropic ray theory and solves the problematic behaviour of S-wave polarizations. We test the application of the prevailing-frequency approximation of the coupling ray theory to 3D ray-based Kirchhoff pre-stack depth scalar migration and compute migrated sections in two simple inhomogeneous weakly anisotropic velocity models composed of two layers separated by a curved interface. The recorded complete seismic wave field is calculated using the Fourier pseudospectral method. We use a scalar imaging for the complete wave field in a single-layer velocity model with the same anisotropy as in the upper layer of the velocity model used to calculate the recorded wave field. We migrate reflected PP, converted PS1 and PS2 elementary waves without the separation of the recorded complete wave field. For migration of the S-wave part we use the prevailing-frequency approximation of the coupling ray theory and for comparison we apply the anisotropic-ray-theory approximation. Calculations using the prevailing-frequency approximation of the coupling ray theory are without problems for both models. On the other hand, for the anisotropic-ray-theory approximation in the model with weaker anisotropy we have to use limitation of Green function maxima otherwise the migrated sections are wrong. In spite of complex recorded wave fields, without decomposition, the migrated interfaces for the vertical component of the PP reflected wave, radial and transversal components of PS1 and PS2 converted waves are in all stacked migrated sections relatively good with exception of spurious interface images close to the correct ones.

KEY WORDS: Fourier pseudospectral method, 3D Kirchhoff pre-stack depth scalar migration, inhomogeneous anisotropic velocity model, weak anisotropy, complete wave field, coupling ray theory.

0963-0651/23/$5.00

INTRODUCTION

It is known that the isotropic ray theory assumes equal velocities of both S-wave polarizations and the anisotropic ray theory assumes both S-wave polarizations strictly decoupled (e.g., Bulant and Klimeš, 2002). The coupling ray theory proposed by Coates and Chapman (1990) provides continuous transition between the isotropic and anisotropic ray theories and solves problematic behaviour of S-wave polarizations in velocity models with weak anisotropy. The isotropic ray theory is applicable to isotropic and very weakly anisotropic media, the anisotropic ray theory is usable for P-waves in all degrees of anisotropy and for S-waves in strongly anisotropic media, the coupling ray theory is applicable to isotropy and to all degrees of anisotropy.

There are many more or less accurate approximations of the coupling ray theory (e.g., Bulant and Klimeš, 2002; Farra and Pšenčík, 2008, 2010; Pšenčík et al., 2012; Klimeš and Bulant, 2016). In this paper, we test the prevailing-frequency approximation of the coupling ray theory (Klimeš and Bulant, 2016). This approach practically eliminates frequency dependence within a limited frequency band and solves the problem in storing the Green function at the nodes of dense grids, typical for applications such as the Born approximation, migrations.

Ray-theory software package ANRAY (Gajewski and Pšenčík, 1990) and packages MODEL, CRT, FORMS (Červený et al., 1988; Bulant, 1996; Bucha and Bulant, 2022) do not offer the possibility to calculate coupling ray-theory S-waves in models with interfaces. In order to compute recorded wave field in inhomogeneous weakly anisotropic model with interface, we used the Fourier pseudospectral method (Tessmer, 1995). The method enables to calculate synthetic seismograms (complete wave field) in 3D heterogeneous anisotropic velocity models with interfaces. In the preceding studies Bucha (e.g., 2012, 2013, 2017, 2021) migrated separate ray-theory elementary waves whereas we migrate a complete wave field in this paper.

The dimensions of the velocity model and the shot-receiver configuration are the same as in the previous papers by Bucha (e.g., 2012, 2013, 2017, 2021), where we studied migration sensitivity to incorrect anisotropy, to incorrect gradients of elastic moduli, to incorrect rotation of the tensor of elastic moduli (stiffness tensor) or to the seismogram components. It is well known that omission of anisotropy can lead to false structural interpretation (e.g., Alkhalifah and Larner, 1994; Gray et al., 2001; Alkhalifah, 2006; Behera and Tsvankin, 2009).

To compute the synthetic recorded wave field, we use simple anisotropic velocity models composed of two layers separated by one curved interface that is non-inclined in the direction perpendicular to the source-receiver profiles. The inhomogeneous upper layer is anisotropic and the bottom layer is homogeneous, isotropic. The velocity models for the Fourier pseudospectral method are extended by absorption stripes at the sides.

We then migrate reflected PP, converted PS1 and PS2 elementary waves (without the separation of the complete wave field) using 3D ray-based Kirchhoff pre-stack depth scalar migration in the single-layer inhomogeneous anisotropic velocity models. If we migrate, for example, with the incident P-wave and the back-propagated S2 wave, we speak about migrating the PS2 converted wave. The S-wave part of converted waves is calculated by means of the prevailing-frequency approximation of the coupling ray theory and by the anisotropic-ray-theory approximation for comparison. Under the scalar migration, we understand here the migration of just a single component of the complete recorded elastic wave field. The elastic moduli in the velocity model used for migration correspond to the upper layer of the velocity model in which the synthetic recorded seismograms have been calculated.

For migration we utilize the MODEL, CRT, FORMS and DATA software packages (Červený et al., 1988; Bulant, 1996; Bucha and Bulant, 2022).

ANISOTROPIC VELOCITY MODELS

The dimensions of velocity models and the measurement configuration are derived from the 2D Marmousi model and dataset (Versteeg and Grau, 1991). The recorded wave field is computed in the velocity model composed of two layers separated by one curved interface (see Fig. 1). The medium in the upper layer is inhomogeneous, weakly anisotropic and the bottom layer is homogeneous, isotropic.

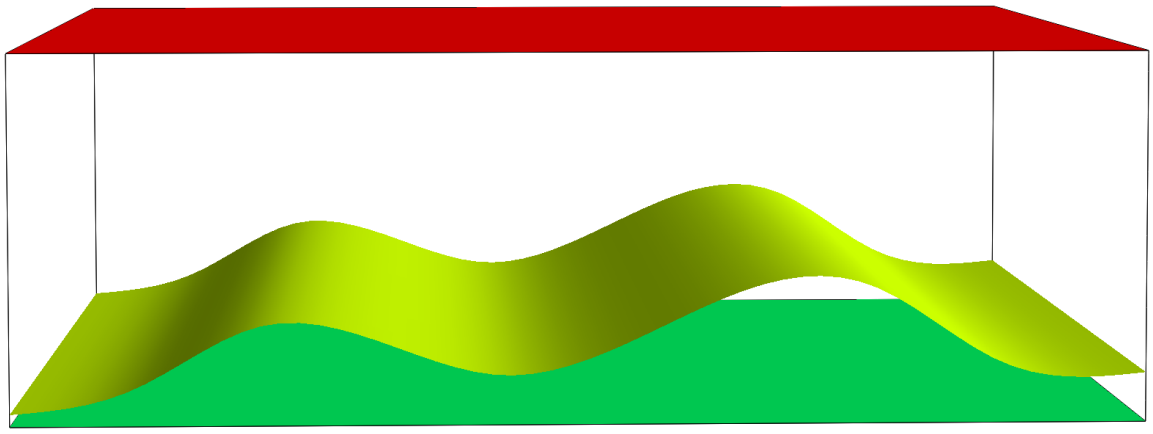

Fig. 1. Velocity model with a curved interface and with inhomogeneous weakly anisotropic upper layer. The horizontal dimensions of the velocity model are 0 km $\leq x_1 \leq$ 9.2 km, 0 km $\leq x_2 \leq$ 10 km and the depth is 0 km $\leq x_3 \leq$ 3 km. The velocity model contains one curved interface which is non-inclined in the direction perpendicular to the source-receiver profiles.

We use anisotropy proposed by Bulant and Klimeš (2008) in the models QI and QI4 for the illustration of coupling effects. The model QI coincides with the WA model of Pšenčík and Dellinger (2001). The model QI was also used by Farra and Pšenčík (2010) for a comparison of the coupling ray theory based on FORT with the standard ray theory results. The QI model is vertically inhomogeneous, transversely isotropic with a horizontal axis of symmetry (HTI). The axis of symmetry is rotated counterclockwise everywhere in the plane (x_1, x_2) by 45° from the x_1 axis. The QI4 model is derived from the QI model and has approximately four times stronger anisotropy.

The matrix of density-reduced elastic moduli of model QI in km^2/s^2 reads at $x_3 = 0$ km:

$$\begin{pmatrix} 14.48500 & 4.52500 & 4.75000 & 0.00000 & 0.00000 & -0.58000 \\ & 14.48500 & 4.75000 & 0.00000 & 0.00000 & -0.58000 \\ & & 15.71000 & 0.00000 & 0.00000 & -0.29000 \\ & & & 5.15500 & -0.17500 & 0.00000 \\ & & & & 5.15500 & 0.00000 \\ & & & & & 5.04500 \end{pmatrix}$$

and at $x_3 = 2.9$ km:

$$\begin{pmatrix} 22.08963 & 6.90063 & 7.24375 & 0.00000 & 0.00000 & -0.88450 \\ & 22.08963 & 7.24375 & 0.00000 & 0.00000 & -0.88450 \\ & & 23.95775 & 0.00000 & 0.00000 & -0.44225 \\ & & & 7.86138 & -0.26688 & 0.00000 \\ & & & & 7.86138 & 0.00000 \\ & & & & & 7.69363 \end{pmatrix} . \qquad (1)$$

The values of anisotropy strength defined as $2(P_{max} - P_{min}) / (P_{max} + P_{min}) \times 100\%$, where P_{min} and P_{max} are minimum and maximum absolute norms of the slowness vector, for model QI are: 8.0% for P-wave, 3.4% for S1 wave and 0.3% for S2 wave.

The matrix of density-reduced elastic moduli of model QI4 in km^2/s^2 reads at $x_3 = 0$ km:

$$\begin{pmatrix} 12.94000 & 3.70000 & 4.60000 & 0.00000 & 0.00000 & -2.32000 \\ & 12.94000 & 4.60000 & 0.00000 & 0.00000 & -2.32000 \\ & & 17.84000 & 0.00000 & 0.00000 & -1.16000 \\ & & & 5.32000 & -0.70000 & 0.00000 \\ & & & & 5.32000 & 0.00000 \\ & & & & & 4.88000 \end{pmatrix}$$

and at $x_3 = 2.9$ km:

$$\begin{pmatrix} 19.35852 & 5.34252 & 6.71500 & 0.00000 & 0.00000 & -3.53800 \\ & 19.35852 & 6.71500 & 0.00000 & 0.00000 & -3.53800 \\ & & 26.83100 & 0.00000 & 0.00000 & -1.76900 \\ & & & 8.07552 & -1.06752 & 0.00000 \\ & & & & 8.07552 & 0.00000 \\ & & & & & 7.40452 \end{pmatrix} . \quad (2)$$

The values of anisotropy strength for model QI4 are: 36.7% for P-wave, 13.4% for S1 wave and 4.5% for S2 wave.

The P-wave velocity in the homogeneous, isotropic bottom layer is $V_p = 3.6$ km/s and the S-wave velocity is $V_s = V_p/\sqrt{3}$. We migrate in the single-layer velocity models (without the curved interface) with the same inhomogeneous anisotropies given by matrices (1) and (2). The elastic moduli in the velocity model for migration correspond to the upper layer of the velocity model in which the synthetic recorded data have been calculated.

We calculate and display slowness and ray-velocity surfaces for anisotropies given by matrices (1) and (2) at the depth $x_3 = 0$ km. The slowness surface (phase-slowness surface, index surface) at spatial point x^m is composed of three sheets corresponding to the three eigenvalues of the Christoffel matrix (Klimeš, 2002). Analogously, the ray-velocity surface (group-velocity surface, Fresnel wave surface) at spatial point x^m is composed of three sheets corresponding to the three eigenvalues of the Christoffel matrix. Fig. 2 shows P, S1 and S2 phase slowness surfaces for QI and QI4 anisotropy. Ray-velocity surfaces are displayed in Fig. 3. Note very close surfaces of S1 and S2 waves for QI anisotropy. The proximity of surfaces causes problems for the ray-theory calculations that are solved by the coupling ray theory.

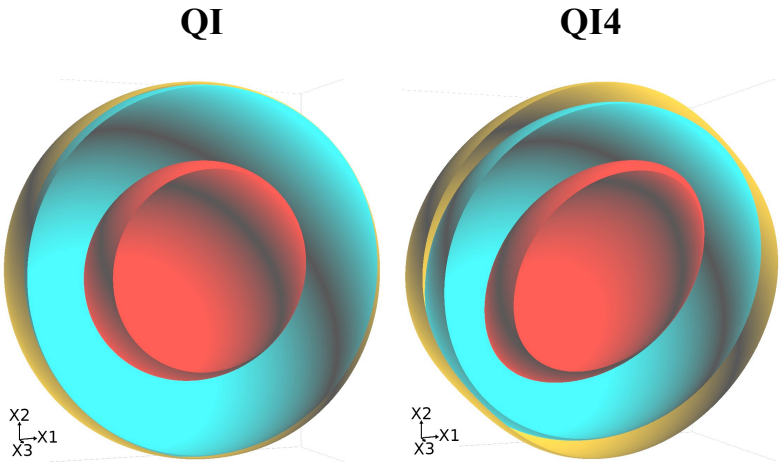

Fig. 2. The P, S1 and S2 wave slowness surfaces for QI and QI4 anisotropy sliced in the plane x_1, x_2. Surfaces are plotted for matrices (1) and (2) at the depth $x_3 = 0$ km.

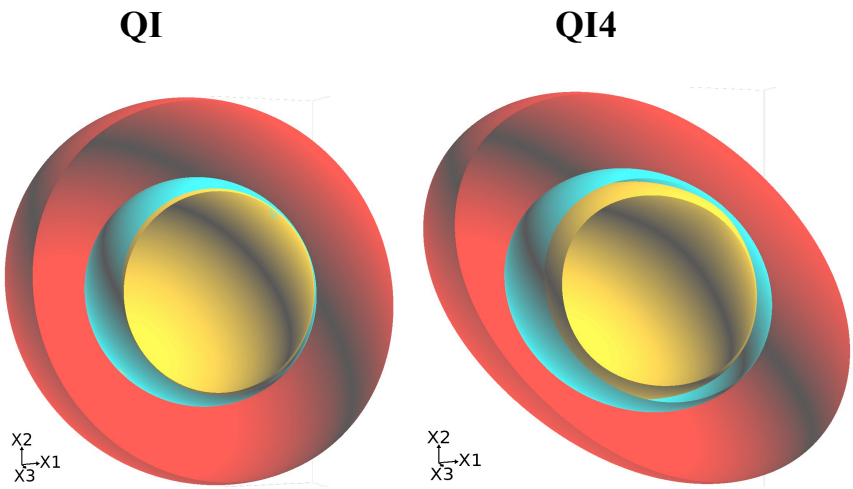

Fig. 3. The P, S1 and S2 wave ray-velocity surfaces for QI and QI4 anisotropy sliced in the plane x_1, x_2. Surfaces are plotted for matrices (1) and (2) at the depth $x_3 = 0$ km.

SHOTS AND RECEIVERS

The profile lines are parallel with the x_1 coordinate axis (see Fig. 4). For each profile line the first shot is 3 km from the left-hand side of the velocity model, the last shot is 8.975 km from the left-hand side of the velocity model, the distance between the shots is 0.025 km, and the depth of the shots is 0 km. The total number of shots along one profile line is 240. The number of receivers per shot is 96, the first receiver is located 2.575 km left of the shot location, the last receiver is 0.2 km left of the shot location, the distance between receivers is 0.025 km, and the depth of the receivers is 0 km. This configuration simulates a simplified towed streamed acquisition geometry. The 3D measurement configuration consists of 81 parallel profile lines. The interval between the parallel profile lines is 0.025 km.

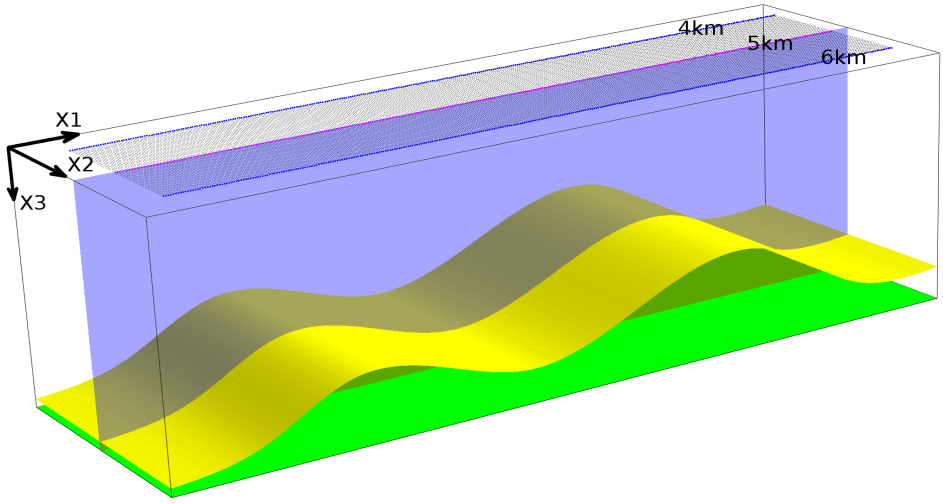

Fig. 4. Part of the velocity model with 81 parallel profile lines, the curved interface (yellow) and the bottom velocity model plane (green). The horizontal dimensions of the depicted part of the velocity model are 0 km $\leq x_1 \leq$ 9.2 km, 3.5 km $\leq x_2 \leq$ 6.5 km, the depth is 0 km $\leq x_3 \leq$ 3 km. We compute and stack migrated sections in the 2D plane (blue) located in the middle of the shot-receiver configuration, at horizontal coordinate x_2 = 5 km.

RECORDED COMPLETE WAVE FIELD

To calculate the recorded complete wave field for 240 shots, we apply code FT43DANX by E. Tessmer (1995). The code is based on the Fourier method (FM), a kind of pseudospectral method (e.g., Kosloff and Baysal, 1982). The code FT43DANX was previously used to test the accuracy of coupling ray theory and standard ray theory results in 3D inhomogeneous, weakly anisotropic media without interfaces (Pšenčík et al., 2012; Bulant et al., 2011). This implementation of the FM is applicable to any type and strength of anisotropy. It works equally well in regular as well as in singular regions of the ray method.

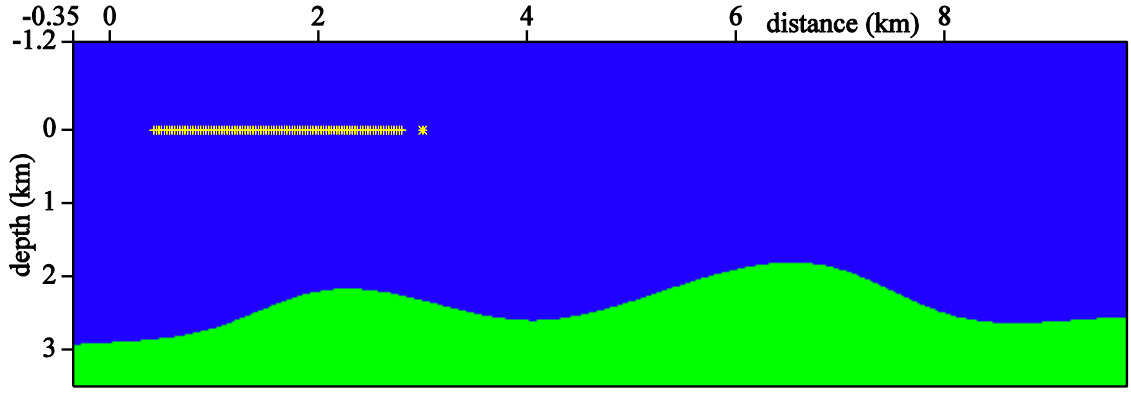

Fig. 5. Section of the enlarged velocity model with 20 absorption grid points for the FM calculation. The dimensions of the section are -0.35 km $\leq x_1 \leq$ 9.75 km and -1.2 km $\leq x_3 \leq$ 3.5 km. The velocity model contains one curved interface which is non-inclined in the direction perpendicular to the source-receiver profiles. The common-shot gather 1 is situated 1.2 km from the top of the enlarged velocity model. The first shot is situated 3.45 km and the first receiver 0.875 km from the left-hand side of the enlarged velocity model. The number of receivers per shot is 96 and the distance between shots and receivers is 0.025 km.

The algorithm is based on a regular numerical grid. For simple structures with horizontal layering, the input parameters for velocity model are located in the main ASCII input file. The velocity model for our tests contains a curved interface. In such a case, the input structure for code FT43DANX needs to be gridded and saved in a separate binary file. We performed gridding of the velocity model using the MODEL and FORMS packages (Červený et al., 1988; Bucha and Bulant, 2022). The code FT43DANX has two limitations for setting grid sizes. The first is that the grid size numbers must be factorizable into the factors up to 23, and the FFT algorithm is the more efficient the smaller factors are. The second limitation is connected with the first one, the grid sizes must be odd numbers. Moreover, numerical algorithms based on pseudospectral methods are computationally more expensive than finite-difference methods. To avoid wrap-around or boundary reflections, the model is surrounded by sponge-like absorbing regions (Cerjan et al., 1985). This requires the numerical grid to be extended at its sides. We present calculation with 20 absorption grid points (recommended lower limit) at the sides of the model. The enlarged

model has numerical grid 405 × 165 × 189 grid nodes in the x_1, x_2 and x_3 directions, respectively. The grid steps are 0.025 km. The horizontal dimensions of the enlarged velocity model are -0.35 km ≤ x_1 ≤ 9.75 km, 0 km ≤ x_2 ≤ 4.1km, and the depth is -1.2 km ≤ x_3 ≤ 3.5 km (see Fig. 5). The grid dimensions of the velocity model are selected with respect to reasonable calculation time on personal computer.

We use an explosive source to calculate the synthetic seismograms. The source-time function is a Gabor wavelet, $\exp[-(2\pi f/\gamma)^2 2t^2] \cos(2\pi ft)$, with the dominant frequency f = 25 Hz and γ = 4. The time step for wave field calculation is 0.003 s and the propagation time starts at 0 s and ends at 2.5 s. The recorded wave field is equal for all parallel profile lines, because the distribution of elastic moduli in the upper layer is vertically inhomogeneous, the bottom layer is homogeneous, and the non-inclined curved interface is independent of the coordinate x_2 perpendicular to the profile lines (2.5D velocity model, see Fig. 4).

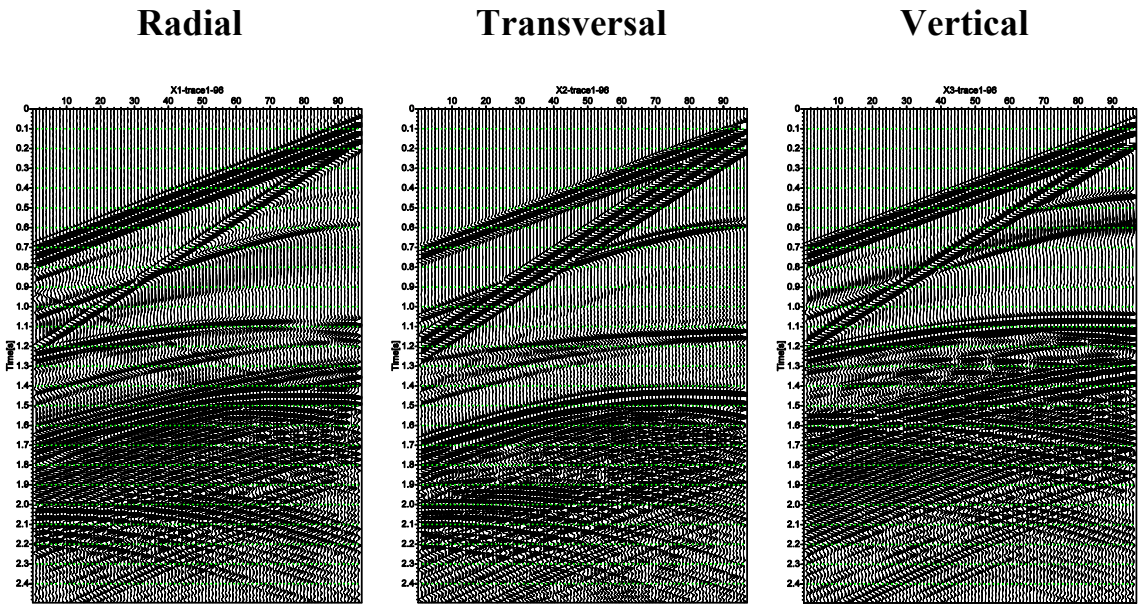

Fig. 6. Radial (X1), transversal (X2) and vertical (X3) components of the complete wave field for common-shot gather 1. The complete seismic wave field is calculated using the Fourier pseudospectral method in the velocity model with the QI anisotropy in the upper layer.

The Fourier method calculates many waves in regions where the ray-theory method fails. For plotting Fourier method (FM) seismograms and snapshots, we use the Seismic Unix plotting tools (Cohen and Stockwell, 2013). To see how complex the complete wave fields are, we display radial (X1), transversal (X2) and vertical (X3) components for common-shot gather 1 calculated in the velocity models with the QI and QI4 anisotropies in the upper layer (see Figs. 6 and 7). Figs. 8 and 9 display radial (X1), transversal (X2) and vertical (X3) snapshots of the wave field for common-shot gather 1. Complete wave fields contain artefacts caused by imperfect absorption stripes at the sides of the velocity model and by diffractions generated at the gridded interface.

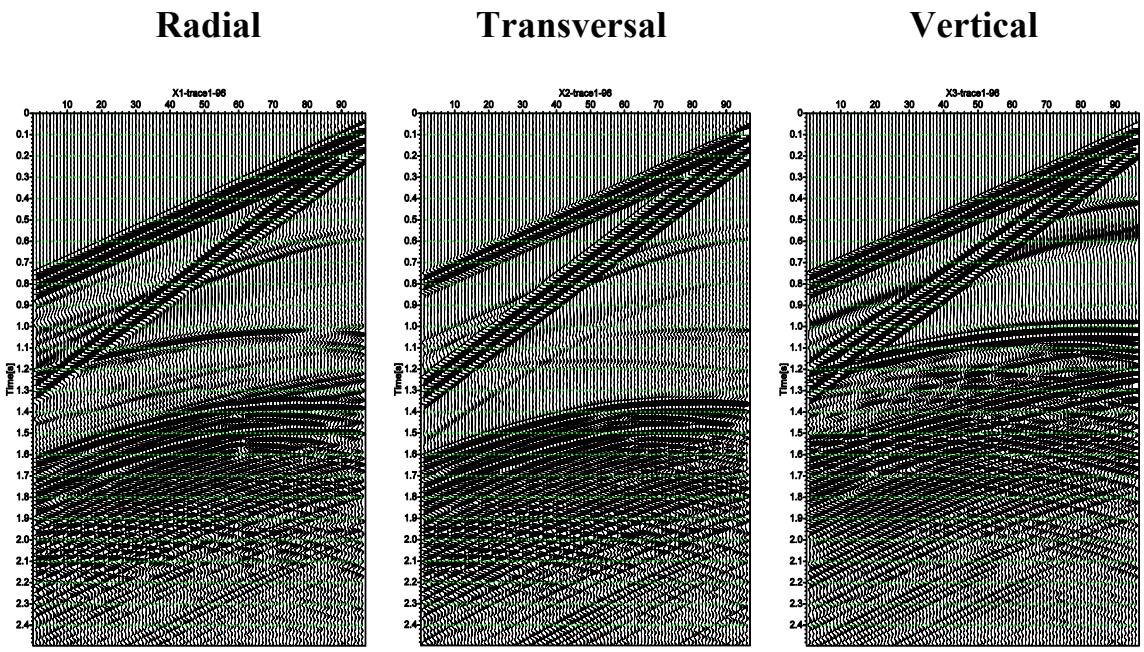

Fig. 7. Radial (X1), transversal (X2) and vertical (X3) components of the complete wave field for common-shot gather 1. The complete seismic wave field is calculated using the Fourier pseudospectral method in the velocity model with the QI4 anisotropy in the upper layer.

KIRCHHOFF PRE-STACK DEPTH SCALAR MIGRATION

We apply the MODEL, CRT, FORMS and DATA software packages for the ray-based 3D Kirchhoff pre-stack depth scalar migration (Červený et al., 1988; Bulant, 1996; Bucha and Bulant, 2022). Under the scalar migration, we understand the migration of a single component of the complete recorded elastic wave field. We migrate the complete wave field without decomposition of elementary waves.

The ray-based migration consists of two-parametric controlled initial-value ray tracing (Bulant, 1999) from the individual surface points, calculating the grid values of travel times and amplitudes by interpolation within ray cells (Bulant and Klimeš, 1999; Klimeš and Bulant, 2017). The paraxial approximation of travel times from the cautiously selected nearest ray (Waheed et al., 2013) is an alternative approach to calculating travel times for migration in inhomogeneous media to avoid interpolation. Then we perform the common-shot Kirchhoff migration and stacking the migrated images. The shot-receiver configuration consists of 81 parallel profile lines at intervals of 0.025 km (see Fig. 4). The first profile line is situated at horizontal coordinate $x_2 = 4$ km and the last profile line is situated at horizontal coordinate $x_2 = 6$ km. For migration we use the single-layer velocity models (without the curved interface) with the same inhomogeneous anisotropies as in the upper layers of the velocity models used to calculate the recorded wave field, given by matrices (1) and (2).

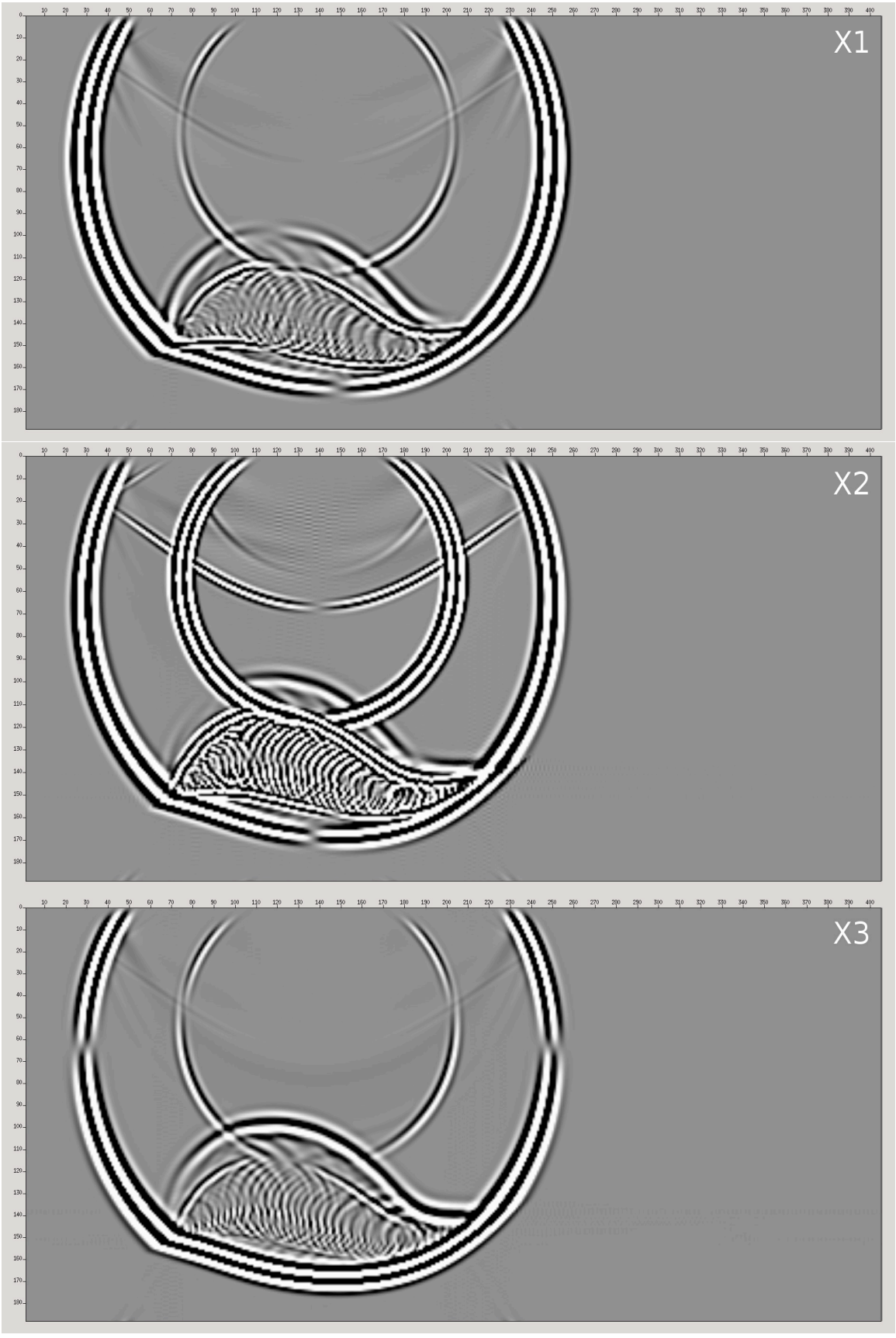

Fig. 8. Snapshots of the radial (X1), transversal (X2) and vertical (X3) components for common-shot gather 1, calculated in the velocity model with the QI anisotropy in the upper layer.

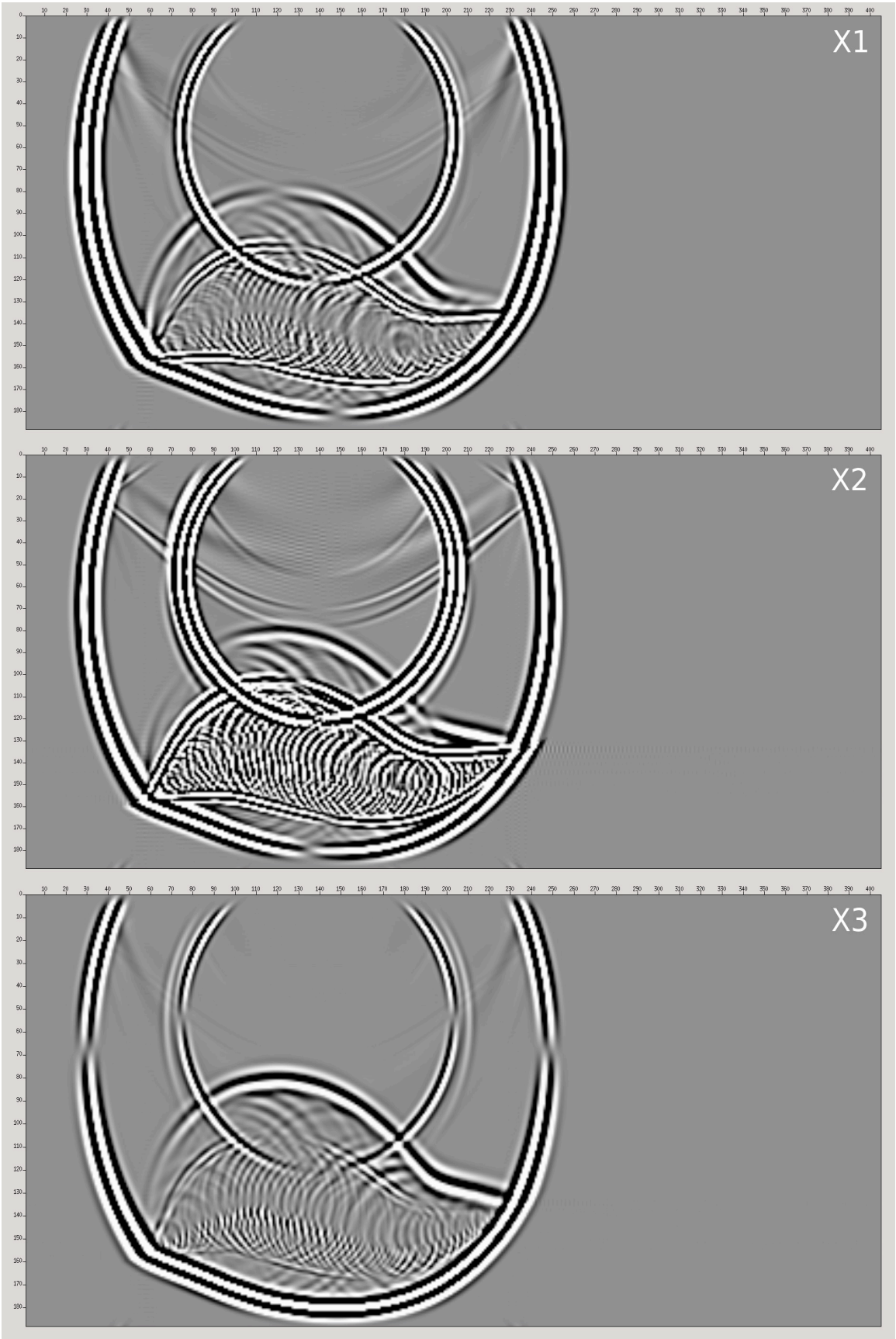

Fig. 9. Snapshots of the radial (X1), transversal (X2) and vertical (X3) components for common-shot gather 1, calculated in the velocity model with the QI4 anisotropy in the upper layer.

In our tests, we calculate only one vertical image section corresponding to the central profile line ($x_2 = 5$ km, see Fig. 4). Although it is only a 2D profile line, such an image represents one vertical section of a full 3D migrated volume. We form the image by computing and summing the corresponding contributions (images) from all 81 parallel source-receiver lines. While summing the contributions, the constructive interference focuses the migrated interface and the destructive interference reduces undesirable migration artefacts (non-specular reflections). We also use cosine taper to clear artefacts, but some of them remain. For inhomogeneous media, we can use travel time compression (e.g., Alkhalifah, 2011), which will also help smooth the traveltime fields to reduce artefacts.

In the ray-based 3D Kirchhoff pre-stack depth scalar migration, we decompose both the incident wave field and the back-propagated wave field into elementary waves P, S1 and S2. We refer to the faster S-wave as the S1 wave, and to the slower S-wave as the S2 wave. If we migrate with the incident P-wave and the back-propagated P-wave, we speak about migrating the PP reflected wave, although we migrate the complete recorded wave field. Analogously, if we migrate with the incident P-wave and the back-propagated S2 wave, we speak about migrating the PS2 converted wave. The migration is tested for three components of the PP reflected wave, PS1 and PS2 converted waves. We calculate the S-wave part of converted PS1 and PS2 waves by means of the prevailing-frequency approximation (PFA) of the coupling ray theory for S-waves (Klimeš and Bulant, 2016) and for comparison we apply the anisotropic-ray-theory approximation (RTA).

The computations are performed in the inhomogeneous weakly anisotropic velocity model QI defined by matrix (1) and in the model QI4 with approximately four times stronger anisotropy defined by matrix (2), respectively. Migrated sections for radial (X1) and transversal (X2) components of PP reflected wave and the vertical component (X3) of PS1 and PS2 converted waves poorly image the migrated interface for both models QI and QI4 so we do not display them. All migrated sections displayed in this paper have stair-step interfaces caused by gridded velocity models. For detailed explanation of the stair-step problem, please refer to Bucha (2019).

DISCUSSION

Figs. 10-14 display stacked sections migrated in the inhomogeneous weakly anisotropic velocity model QI without interface. Fig.10 shows stacked migrated section calculated for the vertical (X3) component of the PP reflected wave. The migrated interface is clear and coincides nearly perfectly with the interface in the velocity model used to compute the recorded wave field.

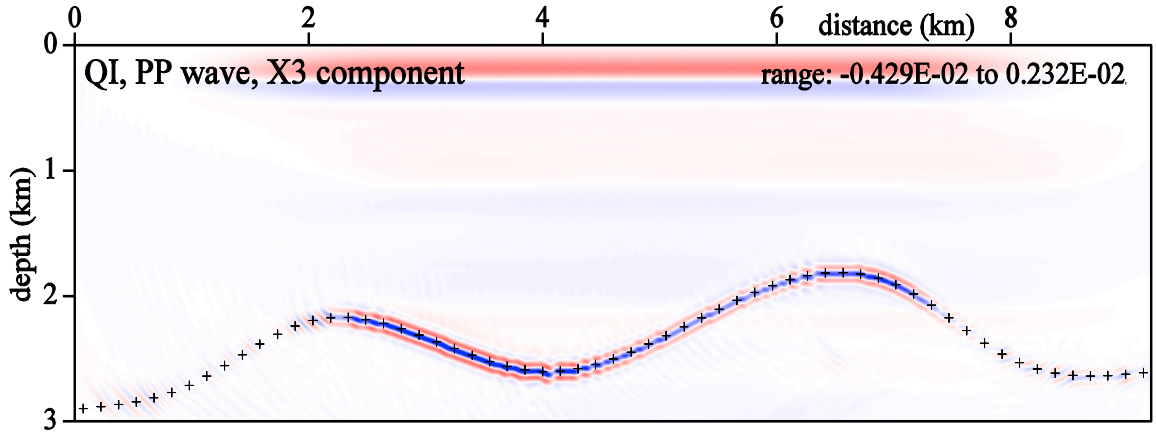

Fig. 10. Stacked section migrated in the weakly anisotropic velocity model QI without interface. The vertical (X3) component of the PP reflected wave is considered. The elastic moduli in the single-layer velocity model for migration are the same as in the upper layer of the velocity model used to calculate the recorded wave field. 81 × 240 common-shot prestack depth migrated sections, corresponding to 81 profile lines and 240 sources along each profile line, have been stacked. The crosses denote the interface in the velocity model used to compute the recorded wave field.

Figs. 11-14 display stacked migrated sections for radial (X1) and transversal (X2) components of PS1 and PS2 converted waves. Although the migrated sections for the prevailing-frequency approximation (PFA) and the anisotropic-ray-theory approximation (RTA) look very similar there are small amplitude differences (PFA-RTA) displayed at the bottom sections of Figs. 11-14. The differences are caused due to different S-wave polarizations between the coupling ray theory and anisotropic ray theory. For comparison note the range of grid values at the right up corners of the migrated sections that are used for setting of the colour scale specific for each section. Red colour corresponds to positive values and blue colour to negative values. The resulting migration interfaces for PFA and RTA are composed of two overlapping interfaces. In comparison with the original interface the false images are slightly shifted downwards (for PS1 wave) or upwards (for PS2 wave). The shift corresponds to the different velocities of PS1 and PS2 waves. In model QI, the velocity differences and the splitting of S1 and S2 waves are very small in comparison with model QI4.

In applying the anisotropic-ray-theory approximation (RTA) to velocity model QI, we encounter problems with anomalous amplitudes of the Green function for PS1 and PS2 waves. These anomalies yield additional migration artefacts (noise) and the migrated interface is not imaged. For example, 24 of 81 profiles for the radial (X1) component of PS1 converted wave are migrated correctly while the rest of profiles has anomalous amplitudes that superimpose the correct interface with anomalous artefacts near the surface of the section (see Fig. 15). We solved the problem by limiting the maximum value of the Green function. However, setting the correct value of the maximum requires additional test calculations. We do not observe the problem with anomalous amplitudes of the Green function for velocity model QI4 with stronger anisotropy.

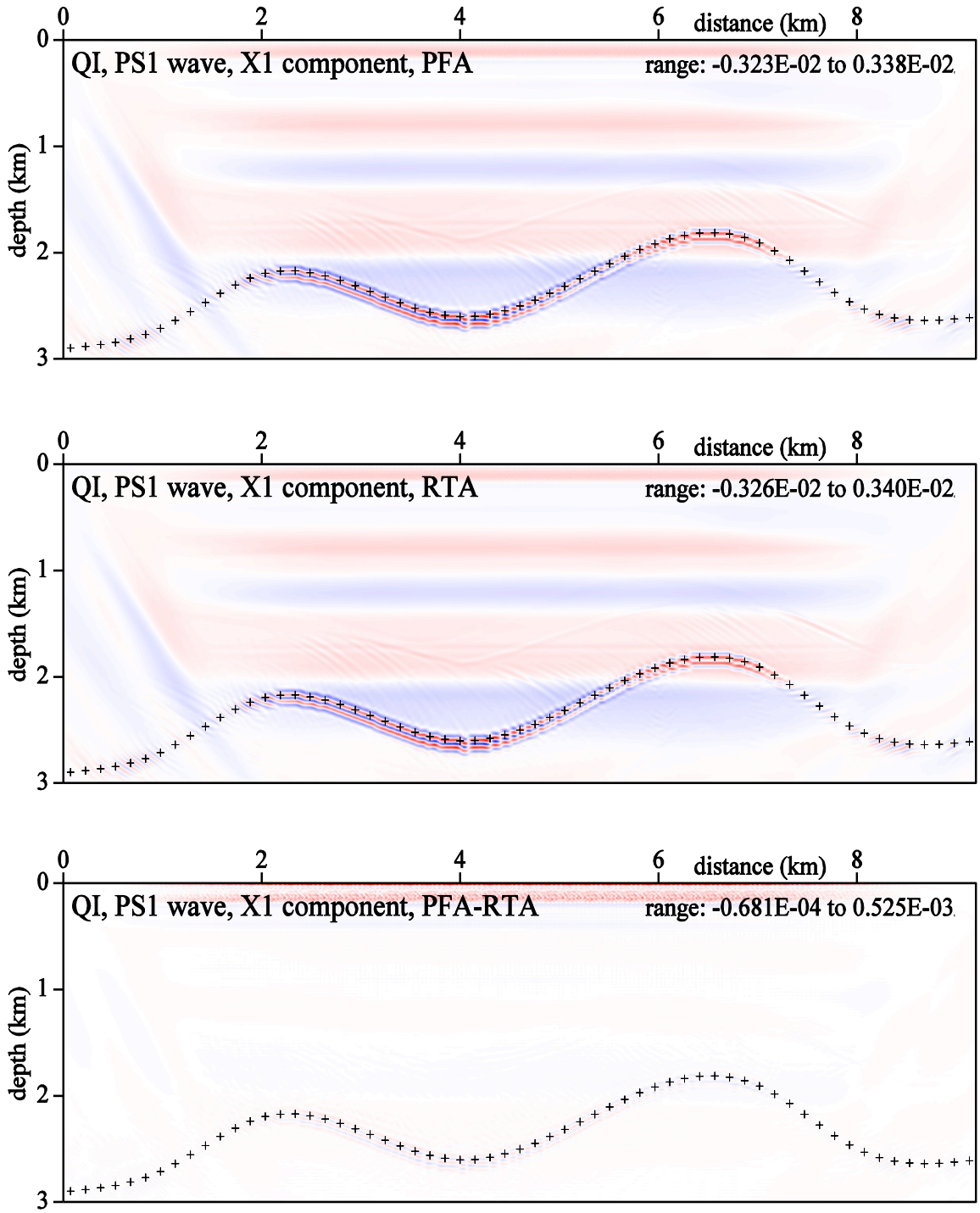

Fig. 11. Stacked sections migrated in the weakly anisotropic velocity model QI without interface. The radial (X1) component of the PS1 converted wave is considered. We compare two approaches for calculation of the S-wave part of the converted PS1 wave: prevailing-frequency approximation (PFA) and anisotropic-ray-theory approximation (RTA). The bottom figure (PFA-RTA) corresponds to subtraction of grid values of the two top figures. The elastic moduli in the single-layer velocity model for migration are the same as in the upper layer of the velocity model used to calculate the recorded wave field. 81 × 240 common-shot prestack depth migrated sections, corresponding to 81 profile lines and 240 sources along each profile line, have been stacked. The crosses denote the interface in the velocity model used to compute the recorded wave field. The top images of the interface in the two top figures (PFA, RTA) are correct, the false images are slightly shifted downwards.

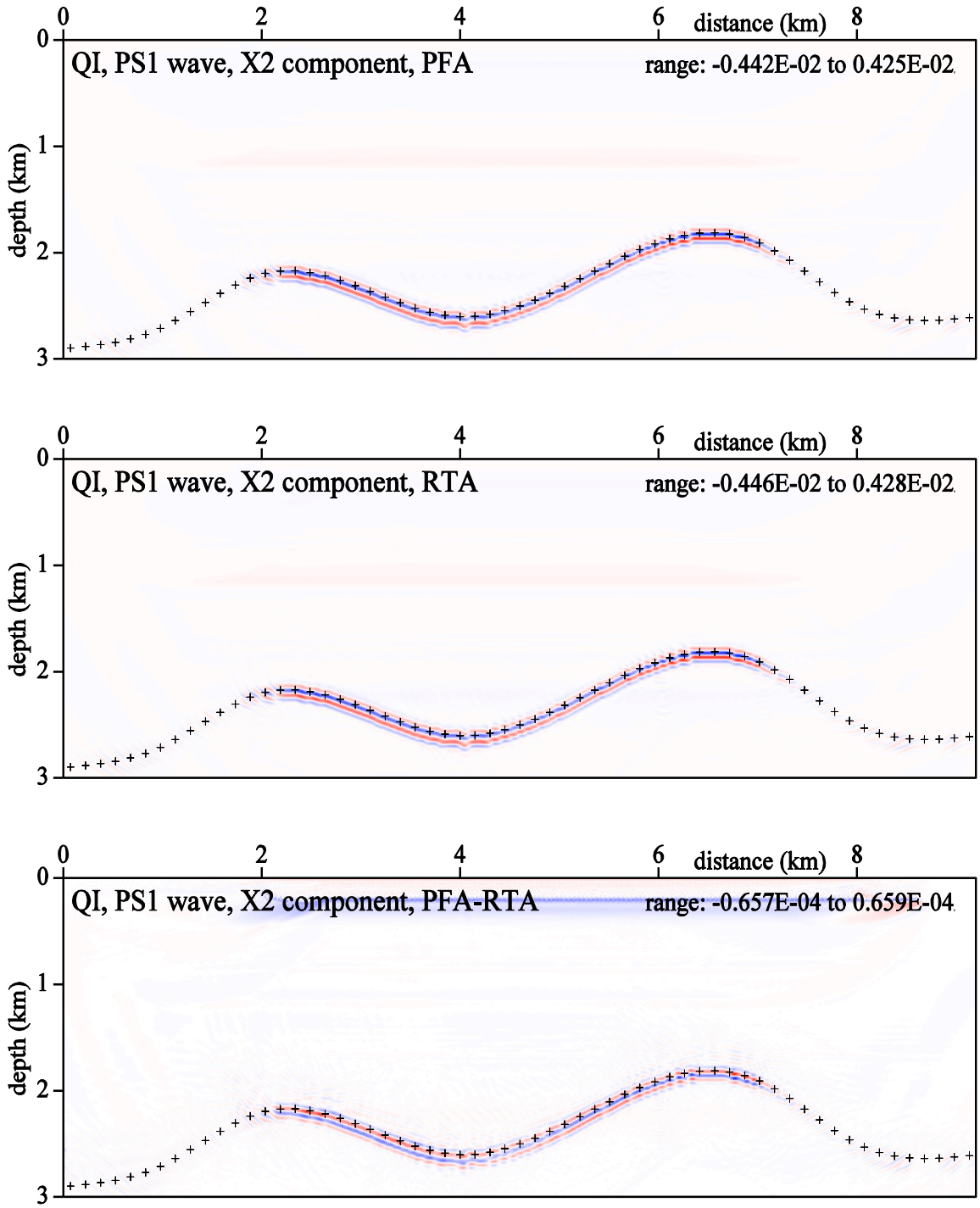

Fig. 12. Stacked sections migrated in the weakly anisotropic velocity model QI without interface. The transversal (X2) component of the PS1 converted wave is considered. We compare two approaches for calculation of the S-wave part of the converted PS1 wave: prevailing-frequency approximation (PFA) and anisotropic-ray-theory approximation (RTA). The bottom figure (PFA-RTA) corresponds to subtraction of grid values of the two top figures. The elastic moduli in the single-layer velocity model for migration are the same as in the upper layer of the velocity model used to calculate the recorded wave field. 81 × 240 common-shot pre-stack depth migrated sections, corresponding to 81 profile lines and 240 sources along each profile line, have been stacked. The crosses denote the interface in the velocity model used to compute the recorded wave field. The top images of the interface in the two top figures (PFA, RTA) are correct, the false images are slightly shifted downwards.

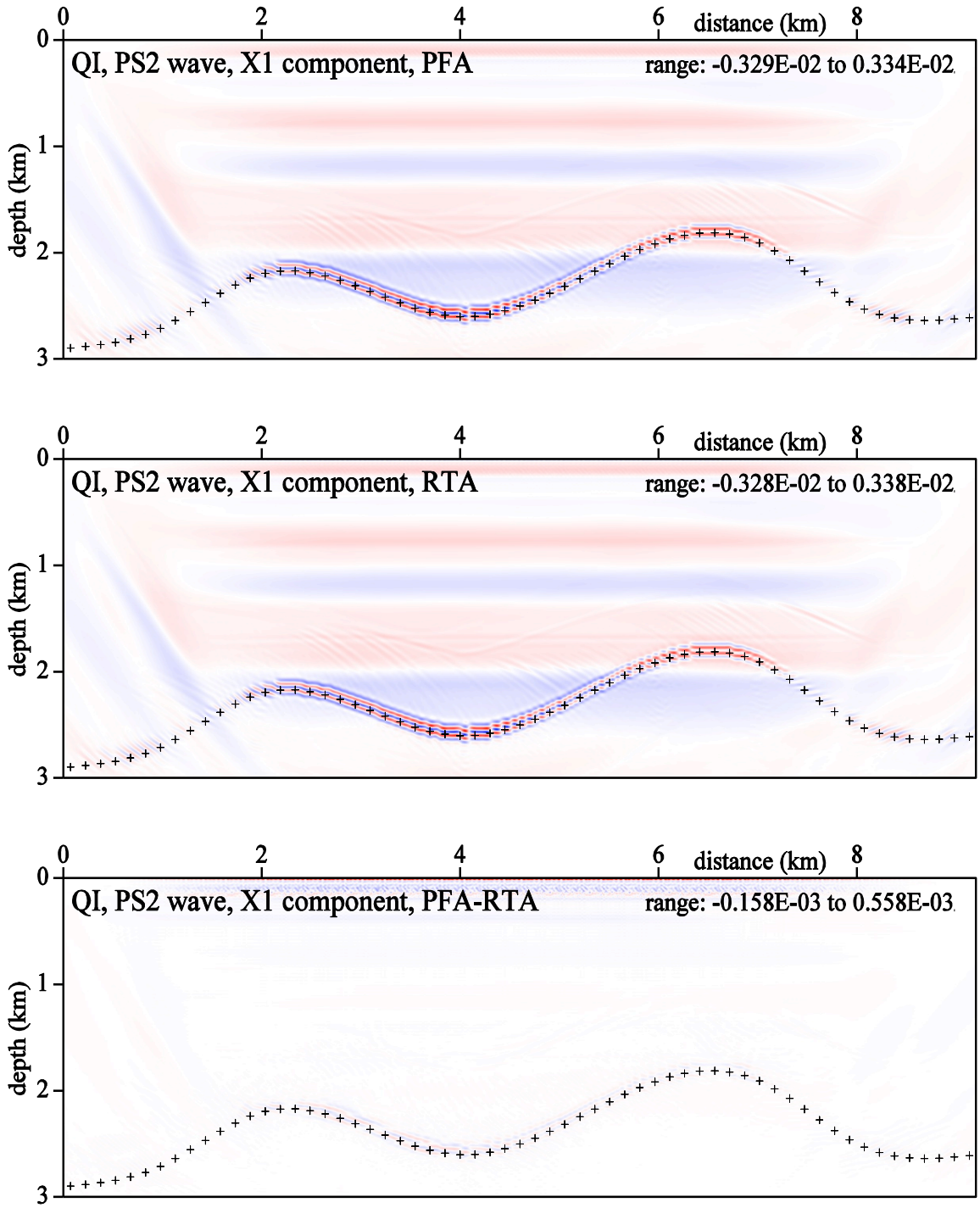

Fig. 13. Stacked sections migrated in the weakly anisotropic velocity model QI without interface. The radial (X1) component of the PS2 converted wave is considered. We compare two approaches for calculation of the S-wave part of the converted PS2 wave: prevailing-frequency approximation (PFA) and anisotropic-ray-theory approximation (RTA). The bottom figure (PFA-RTA) corresponds to subtraction of grid values of the two top figures. The elastic moduli in the single-layer velocity model for migration are the same as in the upper layer of the velocity model used to calculate the recorded wave field. 81 × 240 common-shot pre-stack depth migrated sections, corresponding to 81 profile lines and 240 sources along each profile line, have been stacked. The crosses denote the interface in the velocity model used to compute the recorded wave field. The bottom images of the interface in the two top figures (PFA, RTA) are correct, the false images are slightly shifted upwards.

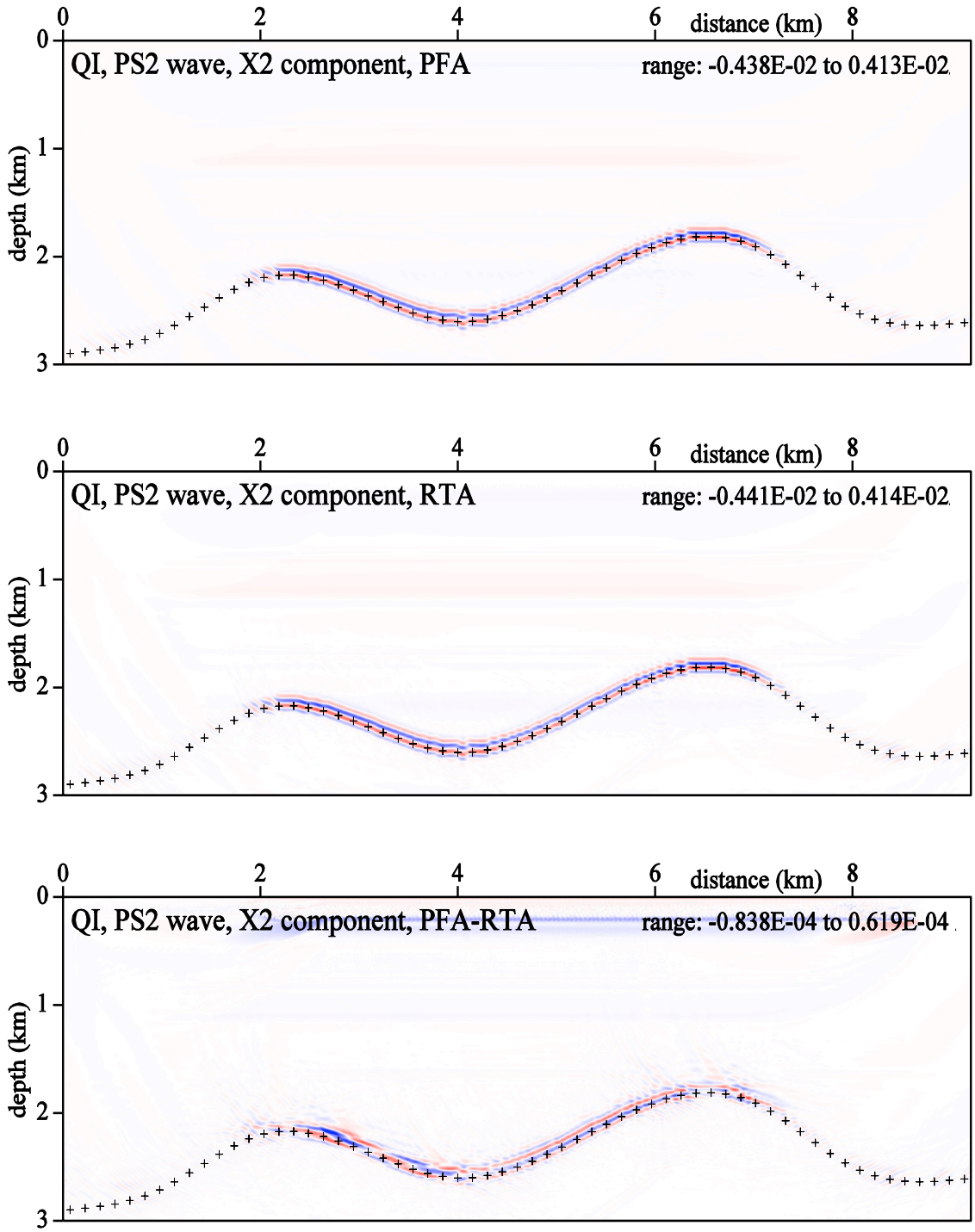

Fig. 14. Stacked sections migrated in the weakly anisotropic velocity model QI without interface. The transversal (X2) component of the PS2 converted wave is considered. We compare two approaches for calculation of the S-wave part of the converted PS2 wave: prevailing-frequency approximation (PFA) and anisotropic-ray-theory approximation (RTA). The bottom figure (PFA-RTA) corresponds to subtraction of grid values of the two top figures. The elastic moduli in the single-layer velocity model for migration are the same as in the upper layer of the velocity model used to calculate the recorded wave field. 81 × 240 common-shot pre-stack depth migrated sections, corresponding to 81 profile lines and 240 sources along each profile line, have been stacked. The crosses denote the interface in the velocity model used to compute the recorded wave field. The bottom images of the interface in the two top figures (PFA, RTA) are correct, the false images are slightly shifted upwards.

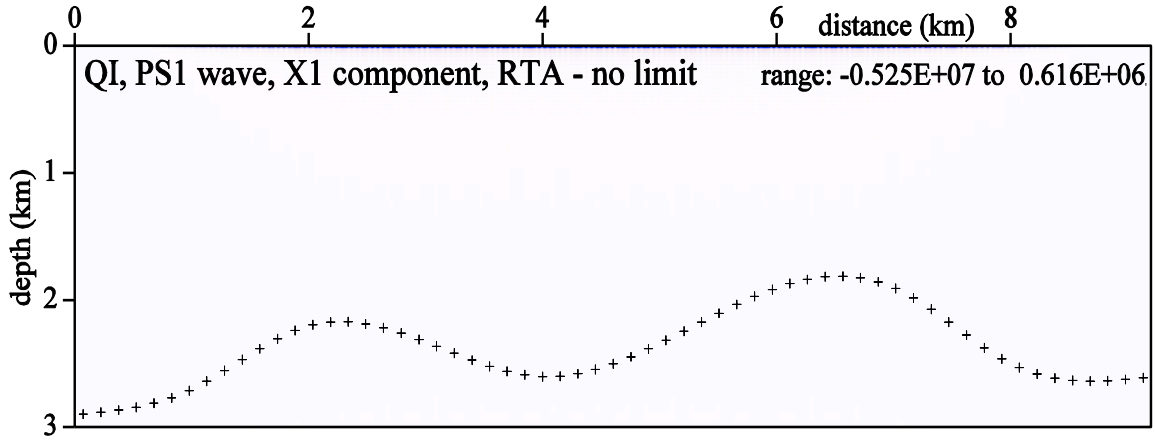

Fig. 15. Stacked section migrated in the anisotropic velocity model QI without interface. The radial (X1) component of the PS1 converted wave is considered. For calculation of the S-wave part of the converted PS1 wave we use anisotropic-ray-theory approximation (RTA) without the limitation of maximum value of the Green function. The elastic moduli in the single-layer velocity model for migration are the same as in the upper layer of the velocity model used to calculate the recorded wave field. 81 × 240 common-shot pre-stack depth migrated sections, corresponding to 81 profile lines and 240 sources along each profile line, have been stacked. The crosses denote the interface in the velocity model used to compute the recorded wave field.

Figs. 16-20 display stacked sections migrated in the inhomogeneous anisotropic velocity model QI4 without interface for PP, PS1 and PS2 waves. The figures are analogous to Figs. 10-14. Stacked migrated section calculated for the vertical (X3) component of the PP reflected wave is clear and coincides nearly perfectly with the original interface (see Fig. 16).

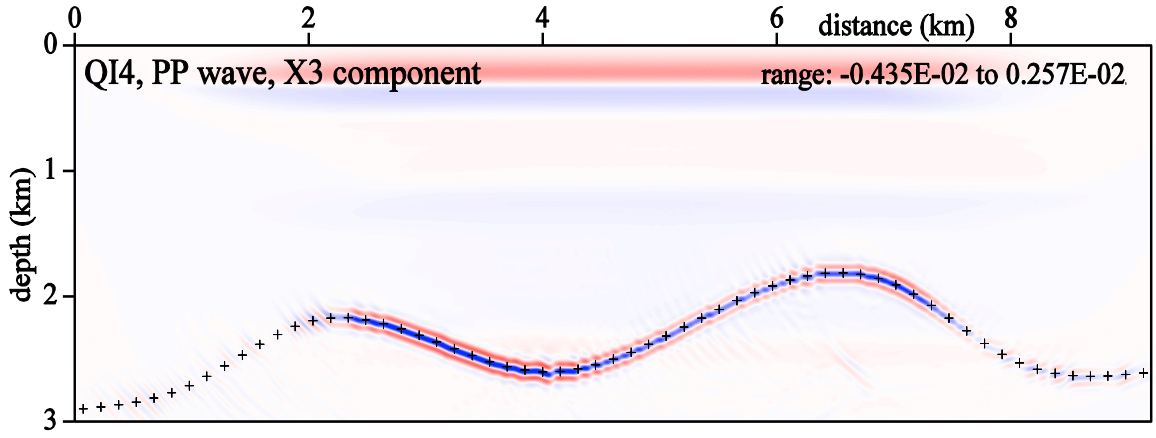

Fig. 16. Stacked section migrated in the anisotropic velocity model QI4 without interface. The vertical (X3) component of the PP reflected wave is considered. The elastic moduli in the single-layer velocity model for migration are the same as in the upper layer of the velocity model used to calculate the recorded wave field. 81 × 240 common-shot pre-stack depth migrated sections, corresponding to 81 profile lines and 240 sources along each profile line, have been stacked. The crosses denote the interface in the velocity model used to compute the recorded wave field.

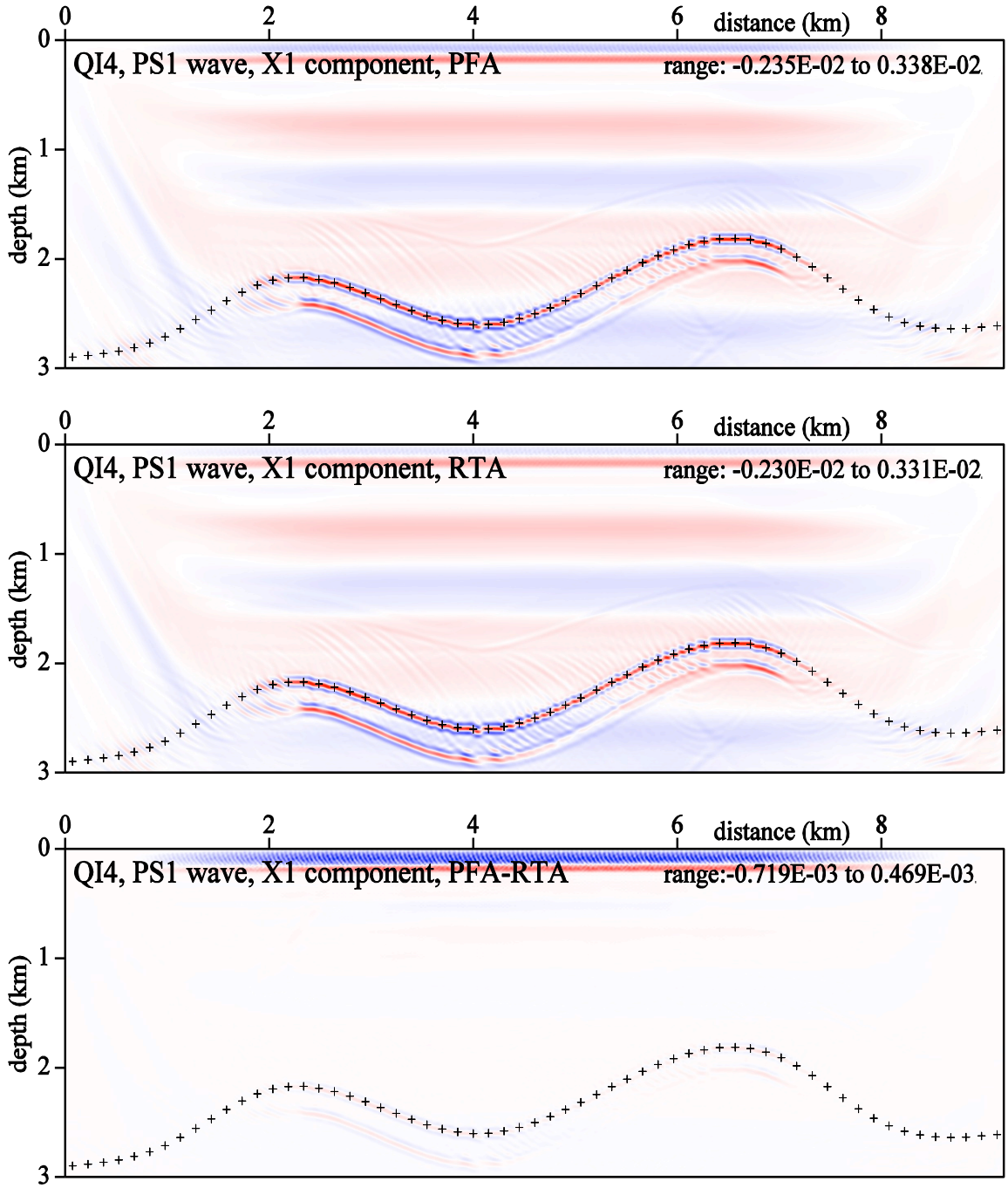

Fig. 17. Stacked sections migrated in the anisotropic velocity model QI4 without interface. The radial (X1) component of the PS1 converted wave is considered. We compare two approaches for calculation of the S-wave part of the converted PS1 wave: prevailing-frequency approximation (PFA) and anisotropic-ray-theory approximation (RTA). The bottom figure (PFA-RTA) corresponds to subtraction of grid values of the two top figures. The elastic moduli in the single-layer velocity model for migration are the same as in the upper layer of the velocity model used to calculate the recorded wave field. 81 × 240 common-shot pre-stack depth migrated sections, corresponding to 81 profile lines and 240 sources along each profile line, have been stacked. The crosses denote the interface in the velocity model used to compute the recorded wave field. The top images of the interface in the two top figures (PFA, RTA) are correct, the false images are displaced downwards.

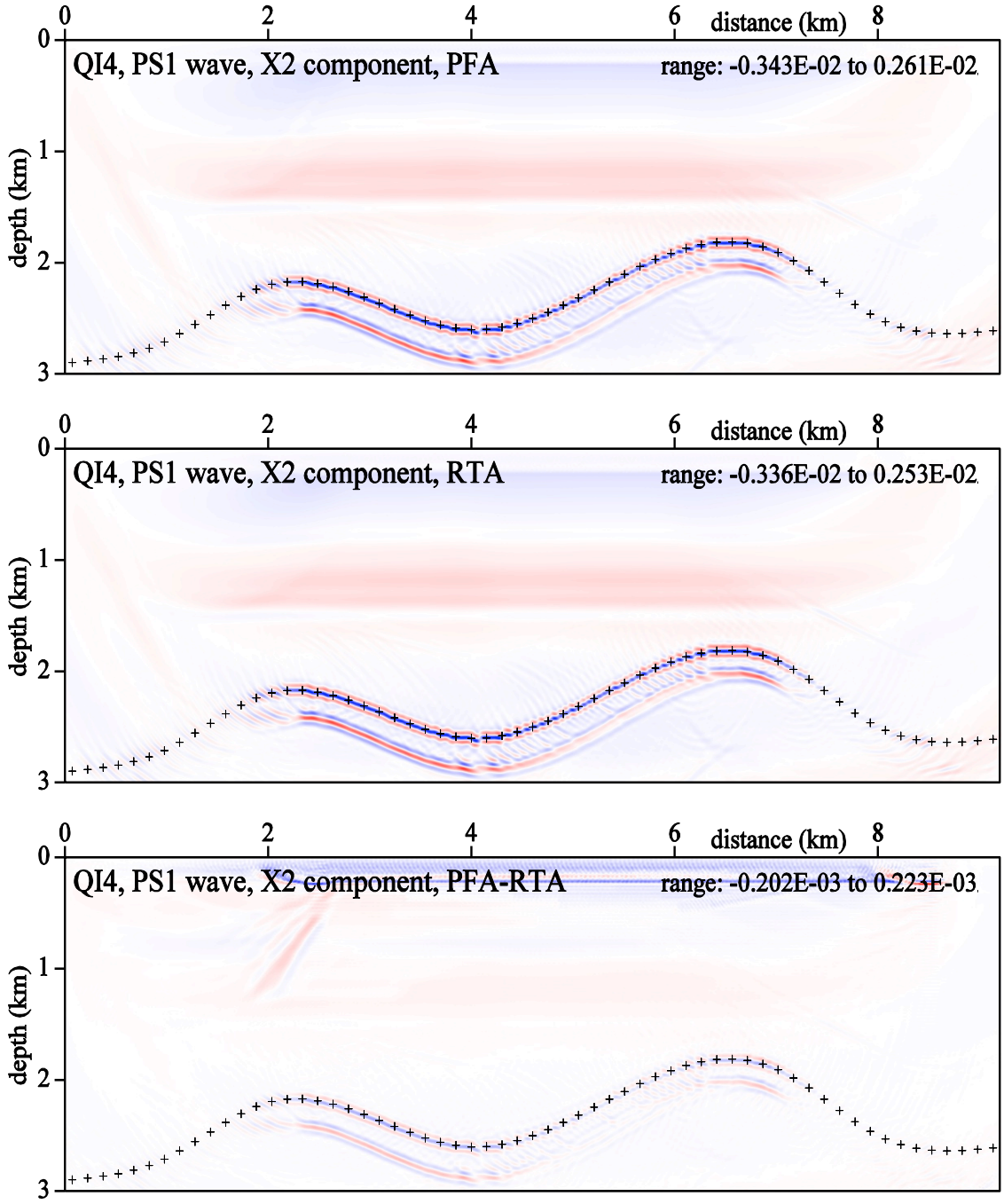

Fig. 18. Stacked sections migrated in the anisotropic velocity model QI4 without interface. The transversal (X2) component of the PS1 converted wave is considered. We compare two approaches for calculation of the S-wave part of the converted PS1 wave: prevailing-frequency approximation (PFA) and anisotropic-ray-theory approximation (RTA). The bottom figure (PFA-RTA) corresponds to subtraction of grid values of the two top figures. The elastic moduli in the single-layer velocity model for migration are the same as in the upper layer of the velocity model used to calculate the recorded wave field. 81 × 240 common-shot pre-stack depth migrated sections, corresponding to 81 profile lines and 240 sources along each profile line, have been stacked. The crosses denote the interface in the velocity model used to compute the recorded wave field. The top images of the interface in the two top figures (PFA, RTA) are correct, the false images are displaced downwards.

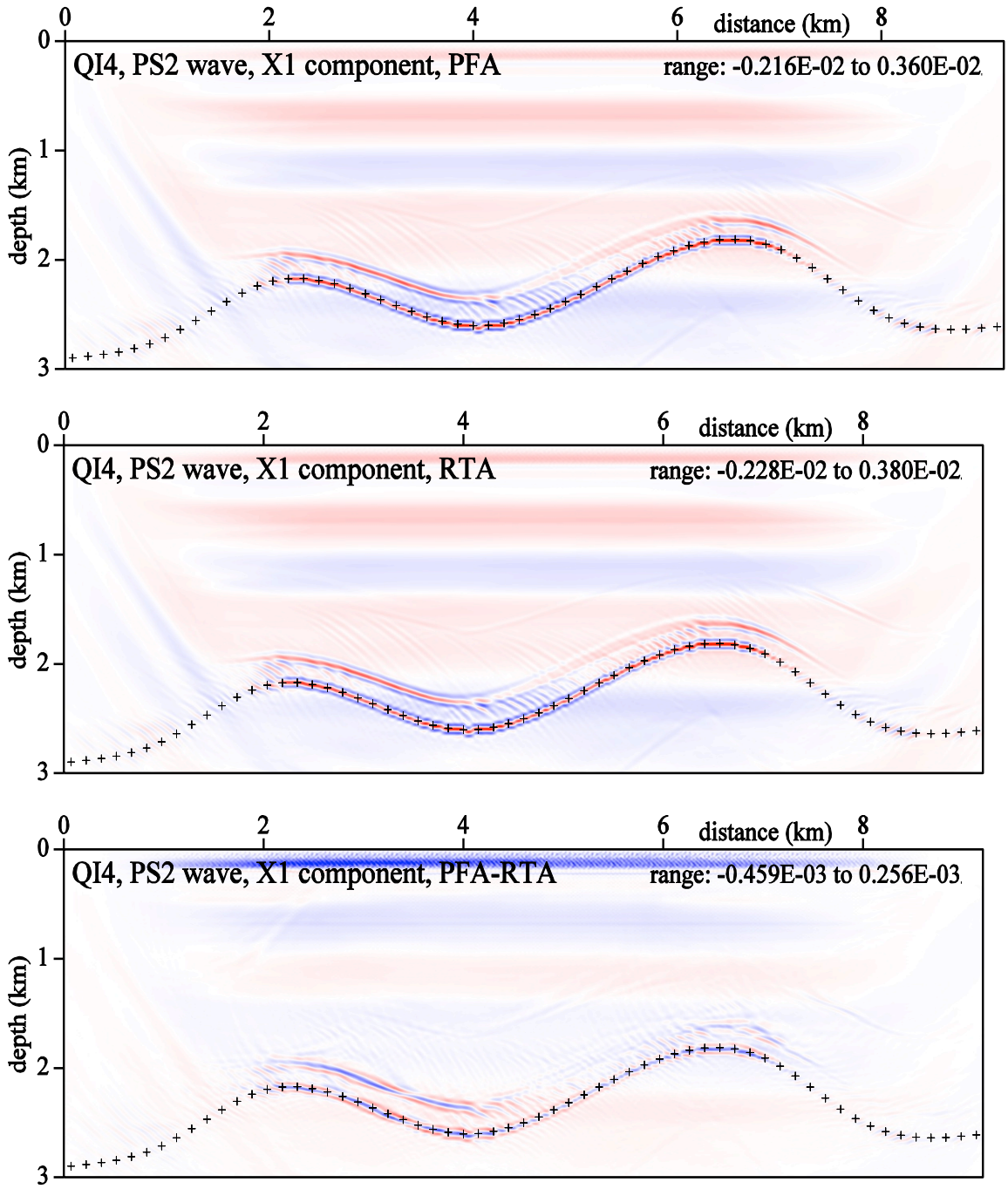

Fig. 19. Stacked sections migrated in the anisotropic velocity model QI4 without interface. The radial (X1) component of the PS2 converted wave is considered. We compare two approaches for calculation of the S-wave part of the converted PS2 wave: prevailing-frequency approximation (PFA) and anisotropic-ray-theory approximation (RTA). The bottom figure (PFA-RTA) corresponds to subtraction of grid values of the two top figures. The elastic moduli in the single-layer velocity model for migration are the same as in the upper layer of the velocity model used to calculate the recorded wave field. 81 × 240 common-shot pre-stack depth migrated sections, corresponding to 81 profile lines and 240 sources along each profile line, have been stacked. The crosses denote the interface in the velocity model used to compute the recorded wave field. The bottom images of the interface in the two top figures (PFA, RTA) are correct, the false images are displaced upwards.

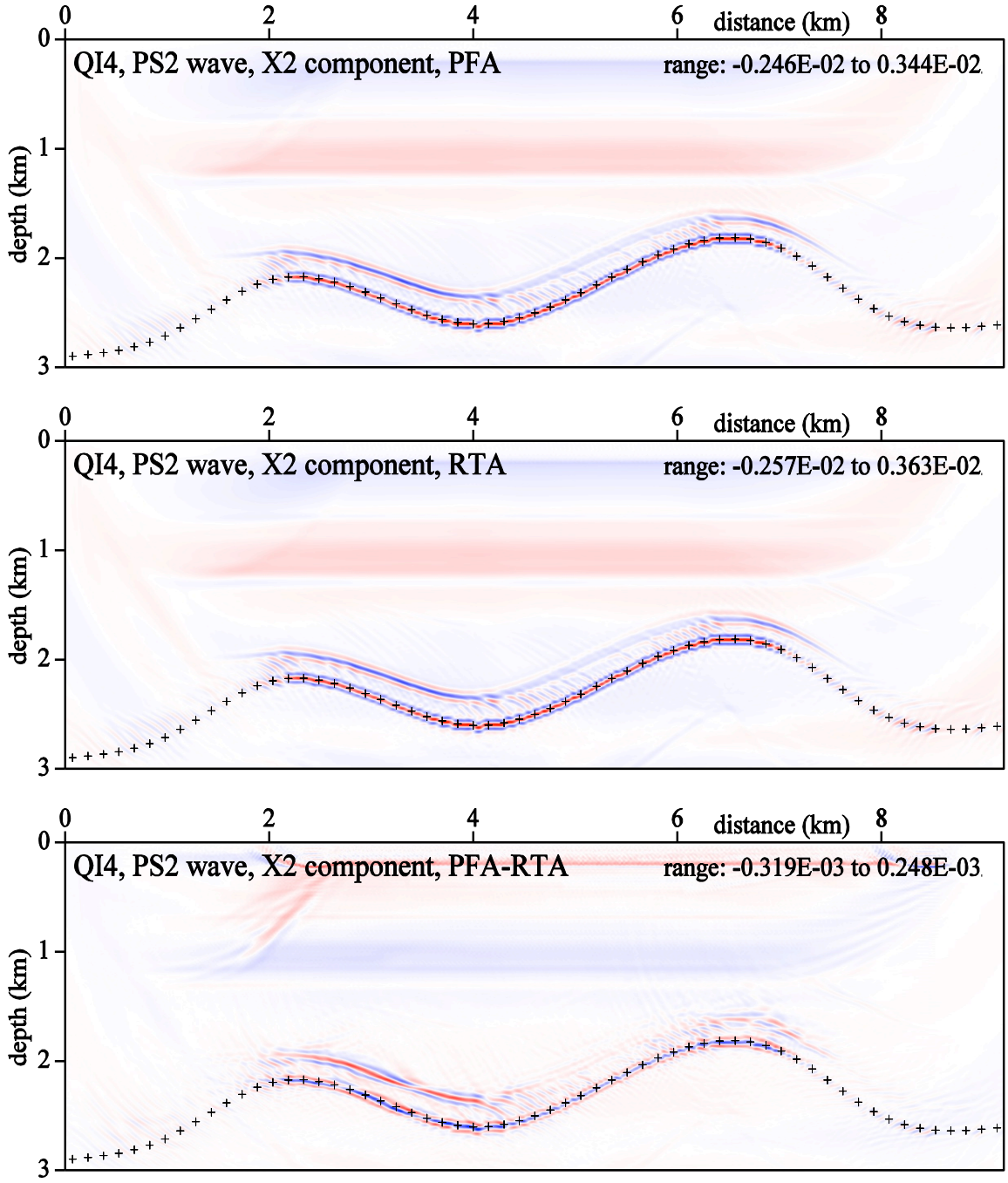

Fig. 20. Stacked sections migrated in the anisotropic velocity model QI4 without interface. The transversal (X2) component of the PS2 converted wave is considered. We compare two approaches for calculation of the S wave part of the converted PS2 wave: prevailing-frequency approximation (PFA) and anisotropic-ray-theory approximation (RTA). The bottom figure (PFA-RTA) corresponds to subtraction of grid values of the two top figures. The elastic moduli in the single-layer velocity model for migration are the same as in the upper layer of the velocity model used to calculate the recorded wave field. 81 × 240 common-shot pre-stack depth migrated sections, corresponding to 81 profile lines and 240 sources along each profile line, have been stacked. The crosses denote the interface in the velocity model used to compute the recorded wave field. The bottom images of the interface in the two top figures (PFA, RTA) are correct, the false images are displaced upwards.

For velocity model QI4, that has approximately four times greater anisotropy than model QI, the splitting of S1 and S2 waves is considerable. Stacked migrated sections in Figs. 17-20 are again nearly equal for two methods of calculating the S-wave part of converted PS1 and PS2 waves, the prevailing-frequency approximation (PFA) and the anisotropic-ray-theory approximation (RTA). Amplitude differences (PFA-RTA) caused by different S-wave polarizations are displayed at the bottom sections. The more pronounced image of the interface corresponds to the converted wave under consideration. The other of the PS1 and PS2 waves generates the spurious image which is unfortunately well visible. The spurious migrated interfaces for PFA and RTA are shifted downwards for the PS1 wave and upwards for the PS2 wave. The shift corresponds to the different velocities of PS1 and PS2 waves.

CONCLUSIONS

We have presented results of the 3D ray-based Kirchhoff pre-stack depth scalar migration of complete wave fields in simple inhomogeneous weakly anisotropic velocity model QI and velocity model QI4 with approximately four times stronger anisotropy. We have migrated reflected PP, converted PS1 and PS2 elementary waves without the separation of the recorded complete wave field. For migration of the S-wave part we have used and compared two methods: the prevailing-frequency approximation of the coupling ray theory and the anisotropic-ray-theory approximation.

Calculations using the prevailing-frequency approximation of the coupling ray theory passed without problems for both models QI and QI4. On the other hand, for the anisotropic-ray-theory approximation in the model QI with weak anisotropy we had to use limitation of Green function maxima, otherwise the migrated sections would be wrong.

In spite of complex recorded wave fields, without decomposition, the migrated interfaces for the vertical component of the PP reflected wave, radial and transversal components of PS1 and PS2 converted waves are in all stacked migrated sections relatively good. The destructive interference reduces and smudges undesirable migration artefacts with exception of spurious interface images close to the correct ones for converted waves.

ACKNOWLEDGEMENTS

The author thanks Ekkehart Tessmer for providing the Fourier method code. The author also thanks Luděk Klimeš and Ivan Pšenčík for their help throughout the work on this paper.

The research has been supported by the Czech Science Foundation under Contract 21-15272J and by the members of the consortium “Seismic Waves in Complex 3-D Structures” (see “http://sw3d.cz”).

REFERENCES

Alkhalifah, T., 2006. Kirchhoff time migration for transversely isotropic media: An application to Trinidad data. Geophysics, 71: S29.

Alkhalifah, T., 2011. Efficient traveltime compression for 3-D prestack Kirchhoff migration. Geophys. Prosp., 59: 1-9.

Alkhalifah, T. and Larner, K., 1994. Migration error in transversely isotropic media. Geophysics, 59: 1405-1418.

Behera, L. and Tsvankin, I., 2009. Migration velocity analysis for tilted transversely isotropic media. Geophys. Prosp., 57: 13-26.

Bucha, V., 2012. Kirchhoff prestack depth migration in 3-D simple models: comparison of triclinic anisotropy with simpler anisotropies. Stud. Geophys. Geod., 56: 533-552.

Bucha, V., 2013. Kirchhoff prestack depth migration in velocity models with and without vertical gradients: Comparison of triclinic anisotropy with simpler anisotropies. In: Seismic Waves in Complex 3-D Structures, Report 23, pp. 45-59, Dept. Geophys., Charles Univ., Prague.

Bucha, V., 2017. Kirchhoff prestack depth migration in simple models with differently rotated elasticity tensor: orthorhombic and triclinic anisotropy. J. Seismic Explor., 26: 1-24.

Bucha, V., 2019. Kirchhoff prestack depth scalar migration of a complete wave field: stair-step interface. Seismic Waves in Complex 3-D Structures, 29: 39-44.

Bucha, V., 2021. Kirchhoff pre-stack depth scalar migration in a simple triclinic velocity model for three-component P, S1, S2 and converted waves. Geophys. Prosp., 69: 269-288.

Bucha, V. and Bulant, P. (Eds.), 2022. SW3D-CD-25 (DVD-ROM). Seismic Waves in Complex 3-D Structures, 31: 89-90.

Bulant, P., 1996. Two-point ray tracing in 3-D. Pure Appl. Geophys., 148: 421-447.

Bulant, P., 1999. Two-point ray-tracing and controlled initial-value ray-tracing in 3-D heterogeneous block structures. J. Seismic Explor., 8: 57-75.

Bulant, P. and Klimeš,, L., 1999. Interpolation of ray-theory travel times within ray cells. Geophys. J. Internat., 139: 273-282.

Bulant, P. and Klimeš,, L., 2002. Numerical algorithm of the coupling ray theory in weakly anisotropic media. Pure Appl. Geophys., 159: 1419-1435.

Bulant, P. and Klimeš, L., 2008. Numerical comparison of the isotropic-common-ray and anisotropic-common-ray approximations of the coupling ray theory. Geophys. J. Internat., 175: 357-374.

Bulant, P., Pšenčík, I., Farra, V. and Tessmer, E., 2011. Comparison of the anisotropic-common-ray approximation of the coupling ray theory for S-waves with the Fourier pseudo-spectral method in weakly anisotropic models. Seismic Waves in Complex 3-D Structures. Report 21: 167-183, Dept. Geophys., Charles Univ., Prague.

Cerjan, C., Kosloff, D., Kosloff, R. and Reshef, M., 1985. A non-reflecting boundary condition for discrete acoustic and elastic wave calculation. Geophysics, 50: 705-708.

Červený, V., Klimeš, L. and Pšenčík, I., 1988. Complete seismic-ray tracing in three-dimensional structures. In: Doornbos, D.J. (Ed.), Seismological Algorithms. Academic Press Inc., New York: 89-168.

Coates, R.T. and Chapman, C.H., 1990. Quasi-shear wave coupling in weakly anisotropic 3-D media. Geophys. J. Internat., 103: 301-320.

Cohen, J.K. and Stockwell, Jr. J.W., 2013. CWP/SU: Seismic Un*x Release No. 43R5: an open source software package for seismic research and processing, Center for Wave Phenomena, Colorado School of Mines, Goldn.

Farra, V. and Pšenčík, I., 2008. First-order ray computations of coupled S-waves in inhomogeneous weakly anisotropic media. Geophys. J. Internat., 173: 979-989.

Farra, V. and Pšenčík, I., 2010. Coupled S-waves in inhomogeneous weakly anisotropic media using first-order ray tracing. Geophys. J. Internat., 180: 405-417.

Gajewski, D. and Pšenčík, I., 1990. Vertical seismic profile synthetics by dynamic ray tracing in laterally varying layered anisotropic structures. J. Geophys. Res., 95B: 11301-11315.

Gray, S.H., Etgen, J., Dellinger, J. and Whitmore, D., 2001. Seismic migration problems and solutions. Geophysics, 66: 1622-1640.

Klimeš, L., 2002. Relation of the wave-propagation metric tensor to the curvatures of the slowness and ray-velocity surfaces. Stud. Geophys. Geod., 46: 589-597.

Klimeš, L. and Bulant, P., 2016. Prevailing-frequency approximation of the coupling ray theory for electromagnetic waves or elastic S-waves. Stud. Geophys. Geod., 60: 419-450.

Klimeš, L. and Bulant, P., 2017. Interpolation of the coupling-ray-theory Green function within ray cells. Stud. Geophys. Geod., 61: 541-559.

Kosloff, D. and Baysal, E., 1982. Forward modeling by a Fourier method. Geophysics, 47: 1402-1412.

Pšenčík, I. and Dellinger, J., 2001. Quasi-shear waves in inhomogeneous weakly anisotropic media by the quasi-isotropic approach: a model study. Geophysics, 66: 308-319.

Pšenčík, I., Farra, V. and Tessmer, E., 2012. Comparison of the FORT approximation of the coupling ray theory with the Fourier pseudospectral method. Stud. Geophys. Geod., 56: 35-64.

Tessmer, E., 1995. 3-D seismic modeling of general material anisotropy in the presence of the free surface by a Chebychev spectral method. Geophys. J. Internat., 121: 557-575.

Versteeg, R.J. and Grau, G. (Eds.), 1991. The Marmousi experience. Proc. EAGE workshop on Practical Aspects of Seismic Data Inversion (Copenhagen, 1990). EAEG, Zeist.

Waheed, U., Pšenčík, I., Červený, V., Iversen, E. and Alkhalifah, T., 2013. Two-point paraxial traveltime formula for inhomogeneous isotropic and anisotropic media: tests of accuracy. Geophysics, 78(5): C41-C56.